Cellulose (2012) 19:1209–1223
DOI 10.1007/s10570-012-9726-0

ORIGINAL PAPER

# Nanofibrillated cellulose (NFC) reinforced polyvinyl alcohol (PVOH) nanocomposites: properties, solubility of carbon dioxide, and foaming

**Yottha Srithep • Lih-Sheng Turng • Ronald Sabo • Craig Clemons**

Received 26 January 2012/Accepted: 14 May 2012/Published online: 26 May 2012


**Abstract** Polyvinyl alcohol (PVOH) and its nanofibrillated cellulose (NFC) reinforced nanocomposites were produced and foamed and its properties—such as the dynamic mechanical properties, crystallization behavior, and solubility of carbon dioxide ($CO_2$)—were evaluated. PVOH was mixed with an NFC fiber suspension in water followed by casting. Transmission electron microscopy (TEM) images, as well as the optical transparency of the films, revealed that the NFC fibers dispersed well in the resulting PVOH/NFC nanocomposites. Adding NFC increased the tensile modulus of the PVOH/NFC nanocomposites nearly threefold. Differential scanning calorimetry (DSC) analysis showed that the NFC served as a nucleating agent, promoting the early onset of crystallization. However, high NFC content also led to greater thermal degradation of the PVOH matrix. PVOH/NFC nanocomposites were sensitive to moisture content and dynamic mechanical analysis (DMA) tests showed that, at room temperature, the storage modulus increased with decreasing moisture content. The solubility of $CO_2$ in the PVOH/NFC nanocomposites depended on their moisture content and decreased with the addition of NFC. Moreover, the desorption diffusivity increased as more NFC was added. Finally, the foaming behavior of the PVOH/NFC nanocomposites was studied using $CO_2$ and/or water as the physical foaming agent(s) in a batch foaming process. Only samples with a high moisture content were able to foam with $CO_2$. Furthermore, the PVOH/NFC nanocomposites exhibited finer and more anisotropic cell morphologies than the neat PVOH films. In the absence of moisture, no foaming was observed in the $CO_2$-saturated neat PVOH or PVOH/NFC nanocomposite samples.

**Keywords** Nanofibrillated cellulose (NFC) · Polyvinyl alcohol (PVOH) · Nanocomposites · Foaming

Y. Srithep · L.-S. Turng (✉)
University of Wisconsin–Madison, Madison, WI, USA
e-mail: turng@engr.wisc.edu

R. Sabo · C. Clemons
U.S. Forest Service, Forest Products Laboratory, Madison, WI, USA

## Introduction

In recent years, environmental concerns have led to an increased interest in natural fibers and biodegradable polymers. At the same time, new technologies originating from the fields of nanotechnology and nanocomposites have led to opportunities in many areas, including materials from forest products (Ahola 2008). Cellulose microfibrils (MFs), which are ordered uniquely in each of the cell wall layers of wood, are tightly bound by multiple hydrogen bonds. Mechanical homogenization or shearing of aqueous

suspensions of cellulose has been used to break many of the bonds, often after chemical or enzymatic pretreatment, resulting in microfibrillated and even nanofibrillated cellulose (NFC) if sufficient energy is applied (Nakagaito and Yano 2004; Andresen et al. 2006; Iwamoto et al. 2007; Alemdar and Sain 2008).

NFC is gaining attention as a reinforcing filler in thermoplastic matrices due to its numerous advantages, which include low density, renewability, high specific properties, biodegradability, gas barrier properties, and unlimited availability (Siqueira et al. 2010; Dufresne et al. 1997; Jonoobi et al. 2010). Despite these attractive properties, the processing temperature of these composites is restricted to about 200 °C due to NFC degradation beyond this temperature, thus restricting the type of matrix that can be used. For instance, polycarbonate (PC) and polyamide (PA) are typically processed at above 240 °C (Samir et al. 2005; Osswald 2006).

In this study, polyvinyl alcohol (PVOH), a biodegradable, water-soluble polymer, was chosen as a matrix for cellulose-reinforced nanocomposites since NFC production usually yields an aqueous gel. Moreover, both PVOH and NFC are known for their good gas barrier properties (Syverud and Stenius 2009; Sanchez-Garcia and Lagaron 2010; Tang and Alavi 2011; Labuschagne et al. 2008). Low polarity gas molecules, such as oxygen and carbon dioxide, exhibit only weak interactions with the highly polar hydroxyl groups in PVOH, resulting in its superior gas barrier properties (Stem et al. 1987). When there are no pores to allow for gas flow through a material, gas permeability will depend on the dissolution of the gas and its rate of diffusion in the particular material (Syverud and Stenius 2009). However, no study has investigated the sorption of $CO_2$ in PVOH and PVOH/NFC nanocomposites. Therefore, we measured the solubility of $CO_2$ in PVOH and PVOH/NFC nanocomposites, as well as its foaming behavior.

Polymeric foams find application as materials for thermal and acoustic insulation, energy dissipation, shock protection, packing, etc. (Avella et al. 2011). Due to their small cell size and high cell density, polymeric foams are light weight and offer better thermal insulation compared to solid materials. This study also carried out batch foaming experiments to investigate the influence of NFC on cell size and cell density using $CO_2$ and/or water as the physical foaming agents.

## Experiments

### Materials

NFC was prepared at the U.S. Forest Service, Forest Products Laboratory (Madison, WI) according to a procedure described by Saito and Isogai (Saito et al. 2006). In particular, fully bleached Kraft eucalyptus fibers were oxidized with sodium hypochlorite using tetramethylpiperidine-1-oxy radical (TEMPO) sodium bromide as a catalyst. The TEMPO-mediated oxidation was carried out at a pH of 10 at 25 °C for 3 h. The fibers were then thoroughly washed and refined in a disk refiner with a gap of approximately 200 μm. The coarse fibers were separated by centrifuging at a force of 12,000 G, and the nanofiber dispersion was concentrated to 1 % using ultrafiltration. A final clarification step was performed in which the nanofiber dispersion was passed once through an M-110EH-30 microfluidizer (Microfluidics, Newton, MA) with 200 and 87 μm chambers in series.

Partially hydrolyzed (87–89%) PVOH, Celvol 502®, was purchased from Celanese Chemicals, Ltd (Dallas, TX). It had a weight-average molecular weight ($M_w$) in the range of 13,000–23,000 and a degree of polymerization of 150–300.

### Processing

The NFC gel was diluted with deionized (DI) water. After the NFC was thoroughly dispersed by magnetic stirring for 30 min, water-soluble PVOH was added, and stirring continued for 2 h on a hotplate at 60 °C to dissolve the PVOH, thus enabling the polymer to mix with the cellulose. PVOH solutions of 0, 2.5, 5, and 10 wt% NFC content were prepared and the resultant solutions appeared to be fully transparent. Then, the mixtures were cast in Petri dishes with a diameter of 90 mm and dried at room temperature (about 25 °C) and atmospheric conditions for 7 days. Final film thicknesses were approximately 0.8 mm. Films were then stored at 90 % humidity and 80 °C to equilibrate the moisture content in all films. Prior to mechanical and thermal testing, some of the specimens underwent additional conditioning to remove any extra moisture.

A transmission electron microscope (TEM, LEO 912) was used to characterize the dispersion of NFC.

For dilute NFC–PVOH solutions, a drop was deposited on a carbon-coated TEM grid and allowed to dry prior to imaging. For TEM imaging of nanocomposites, PVOH specimens containing 10 % NFC were cut into 50–70 nm slices via an ultra-microtome at room temperature. Before the sections became clustered, a tweezers was used to separate them and TEM grids were placed on the slices for imaging. The TEM was operated at 120 kV at room temperature.

### Tensile testing

Type V tensile specimens (ASTM D638—standard test method for tensile properties of plastics) were punched from films conditioned at 90 % humidity using a cutting die. Prior to testing, samples were stored for 4 days in the tensile testing room, which was conditioned at 50 % humidity at 25 °C. The static tensile modulus, strength, and strain-at-break were measured on an Instron 5865. Tensile testing was performed on all specimens using an initial load of 2 N and a constant crosshead speed of 10 mm/min.

The experimental data obtained were compared with three theoretical models to predict the Young's modulus of the composite materials. The first model used the classical Rule of Mixtures approach where the Young's Modulus was calculated according to Eq. (1). The other models were the Mean Field approach of Halpin–Kardos (modified rule of mixture), as shown in Eq. (2), and the Percolation approach, as shown in Eq. (3) (Bulota et al. 2011; Davies 1971a).

$$E = E_r X_r + E_m X_m \tag{1}$$

$$E^n = E_r^n X_r + E_m^n X_m \tag{2}$$

Davies suggested that the constant, *n*, be set to 1/5 based on theoretical analyses (Davies 1971b; Allen et al. 1974; Bulota et al. 2011),

$$E = \frac{(1 - 2\psi + X_r)E_m E_r + (1 - X_r)\psi E_r^2}{(1 - X_r)E_r + (X_r - \psi)E_m} \tag{3}$$

where E is the nanocomposite modulus, $E_r$ is the reinforcement modulus (which was assumed to be the same as that of a dried NFC film prepared by evaporating water from the NFC suspension), $E_m$ is the matrix modulus, $X_r$ is the fiber volume fraction, and $X_m$ is the matrix volume fraction. The percolation volume fraction, $\psi$, is given by

$$\psi = \left(\frac{X_r - X_c}{1 - X_c}\right)^b \tag{4}$$

where $X_c$ is a percolation threshold (in this work it was assumed to be 5 % based on the results of Bulota et al. (2011) and b is the critical percolation exponent which is equal to 0.4 for a three-dimensional system (Siqueira et al. 2010).

### Differential scanning calorimetry (DSC)

Differential scanning calorimetry (DSC) was performed on a DSC Q20 (TA Instruments). The specimens used for DSC characterization were taken from the 90 % humidity room to a 30 % humidity room for 4 days prior to DSC testing to reduce the moisture content in the samples. Specimens of 6-8 mg were placed in aluminum sample pans and heated from 30 to 205 °C at a 10 °C/min heating rate and held at 205 °C for 2 min to eliminate any prior thermal history yet minimize degradation. Specimens were then cooled at 10 °C/min to 30 °C. The specimens were then reheated to 205 °C and cooled down to room temperature using the same temperature, holding time, and cooling rates. The crystallization temperature ($T_c$) was determined from the DSC cooling curves.

### Thermogravimetric analysis (TGA)

Samples used for thermogravimetric analysis (TGA) were dried at 90 °C for 2 days. TGA was performed using a TGA Q50 (TA Instruments) from 25 to 600 °C at a heating rate of 10 °C/min. Approximately 10 mg of neat PVOH, neat NFC, or nanocomposites of various NFC contents, were used for each test. The loss of weight was recorded and normalized against the initial weight.

### Dynamic mechanical analysis (DMA)

Dynamic mechanical analysis (DMA) measurements were performed on a DMA Q800 (TA Instruments) in single cantilever mode. The specimens from the 90 % humidity room were cut to approximately 35.2 by 12.7 by 0.8 mm and then kept in the testing room (50 % humidity at 25 °C) for 4 days before the test. During the DMA test, the specimens were heated at a rate of 3 °C/min from –20°C to 150 °C with a frequency of 1 Hz and an amplitude of 50 μm. To study the effect

of moisture content on the dynamic mechanical properties, additional specimens were dried in an oven at 90 °C for 2 days prior to DMA testing for comparison with the equilibrated specimens. The DMA testing took around 1 h. The weight gain due to moisture of the dried samples in 50 % humidity at room temperature was around 0.02 %, which was insignificant.

## Sorption measurement

The main purpose of the sorption experiments was to establish the amount of $CO_2$ absorbed in the PVOH and PVOH/NFC nanocomposites. The original weights of these samples were measured using a digital balance readable to 0.0001 g. Sorption of $CO_2$ was facilitated by placing the specimens in a high-pressure vessel under a $CO_2$ gas pressure of 5.52 MPa (800 psi) at room temperature for 1 day. No further weight gain was detected in samples placed in the pressure vessel for more than 1 day, suggesting that it had reached steady state. Afterward, the vessel was depressurized and the $CO_2$-absorbed samples were removed from the pressure vessel and placed on a balance to record the $CO_2$ sorption in the pressure chamber and its desorption over time at atmospheric pressure. The process of depressurization and removing the samples from the pressure chamber and weighing them took around 40 s. Samples were kept in an oil bath on the scale to reduce weight gain or loss in the sample due to moisture.

## Foam preparation

To study the foaming behavior and the effect of moisture on foaming (i.e., using the absorbed water as the plasticizer and/or physical blowing agent), neat PVOH and its nanocomposites with different moisture contents were foamed in a batch process. The samples were either: (1) pre-conditioned at 90 % humidity for 2 days, or (2) dried in an oven at 90 °C for 2 days.

In the batch foaming process used in this study, ASTM D638 Type V tensile test bars made of neat resin and nanocomposites were punched from the films and then placed in a pressure vessel filled with $CO_2$ at 5.52 MPa (800 psi) for 1 day, allowing ample time for $CO_2$ to diffuse into the samples. When the specimens were removed from the pressure vessel and brought to atmospheric pressure, supersaturated specimens—which were thermodynamically unstable due to the excessive gas dissolved in the polymer—were produced. This resulted in the nucleation and growth of gas microcells. After 2 h at room temperature, the specimens were placed into a hot oil bath at 135 °C for 10 s to vaporize the moisture inside of the specimens. If cells were not first allowed to nucleate and begin to grow for this 2-h time period, placement into a hot oil bath caused severe cracking of the matrix due to the amount of vapor formed.

## Scanning electron microscopy (SEM)

The cryogenically fractured surfaces were examined using an SEM (LEO 1530) operated at 3 kV. The samples were frozen in liquid nitrogen and then fractured using two small pliers. All specimens were sputter-coated with a thin layer of gold (~20 nm) prior to examination.

## Characterization of foams

The densities of the samples were measured by a toluene displacement technique [ASTM D792 (standard test method for density and specific gravity (relative density) of plastics)]. The density of toluene at 20 °C is 868 g/cm$^3$ (Poling et al. 2008). The weights of unfoamed and foamed samples were measured in air ($M_a$) and toluene ($M_T$), and the density was determined by:

$$\text{Density} = 868\left(\frac{M_a}{M_T}\right) \tag{6}$$

The reported density is the average of five replicates.

The average cell size and cell density of the PVOH nanocomposites was quantitatively analyzed using an image analysis tool (UTHSCSA ImageTool). The cell density was calculated using the following formula (Naguib et al. 2002),

$$\text{Celldensity} = \left(\frac{N}{L^2}\right)^{3/2} M \tag{7}$$

where $N$ is the number of cells, L is the linear length of the area, and $M$ is the unit conversion factor resulting in the number of cells per cm$^3$. For cells of irregular shape, the cell size was taken to be the largest opening dimension.

## Results and discussions

### Dispersion of NFC in PVOH

Figure 1a and b show TEM images of a dilute NFC–PVOH solution dried on carbon-coated grids and the ultra-microtomed specimens, respectively. The TEM images illustrate that NFC is an interconnected web with fibrils having a diameter in the range of 10–50nm. When dispersed in water, NFC forms a very stable suspension due to the interfibrillar repulsive forces created during the TEMPO pre-treatment. Based on the TEM images, it was concluded that NFC dispersed well in a PVOH water solution. Further evidence for the uniformity of the dispersion was the full transparency of the resulting films as shown in Fig. 2 (Siró and Plackett 2010).

### Tensile properties

Tensile tests were performed on specimens punched from the cast films. Representative stress–strain

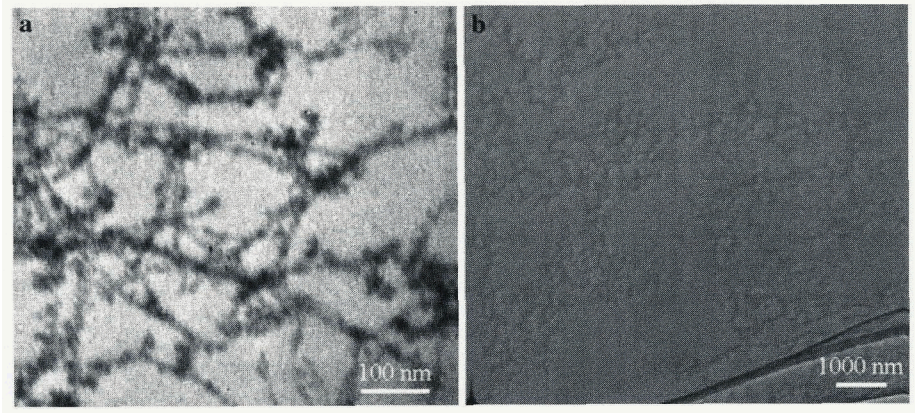


Fig. 1 TEM images for nanocomposites. **a** Sample was obtained by evaporating an NFC and PVOH water solution on a carbon-coated grid. b Sample was obtained by cutting via ultra-microtome. *Scale bars* are 100 nm and 1,000 nm for (**a**) and (**b**), respectively

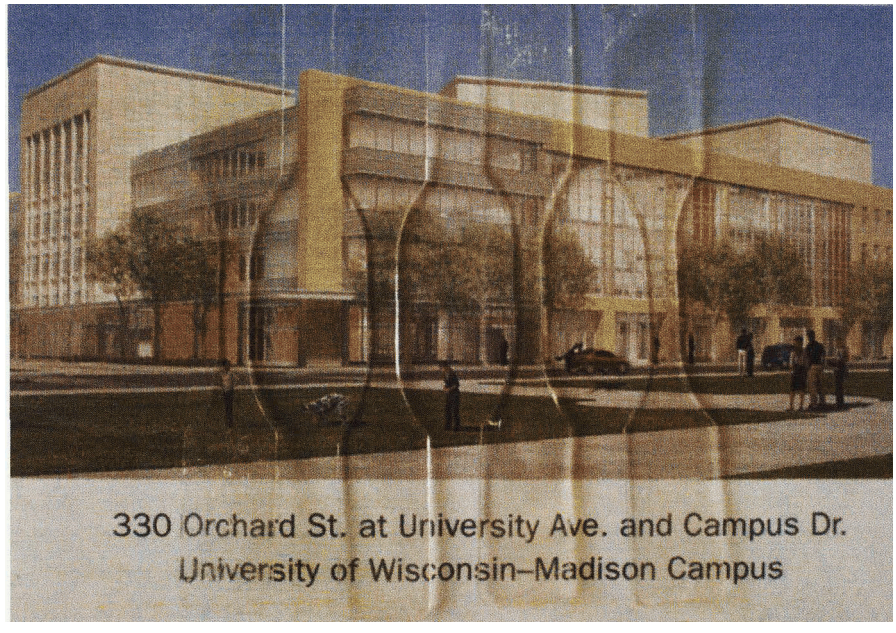


Fig. 2 Transparency (from *left* to *right*) of neat PVOH and PVOH/NFC nanocomposites with 2.5, 5, and 10 % NFC, respectively

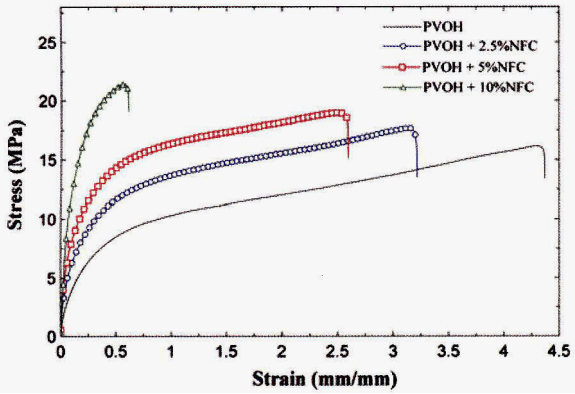


**Fig. 3** Tensile stress versus strain curve for the NFC and PVOH nanocomposites

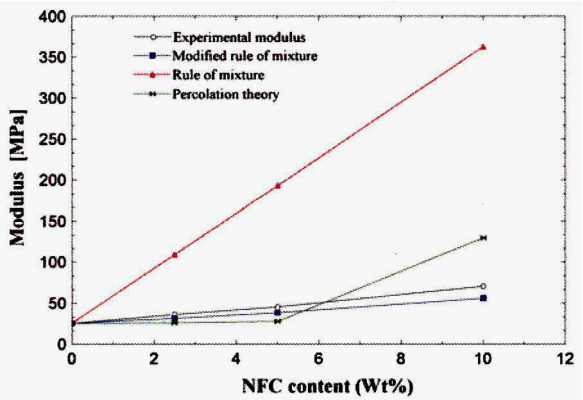


**Fig. 4** Comparison of experimental data to models

curves are featured in Fig. 3. The addition of NFC yielded stronger and stiffer composites but toughness (measured as work of fracture) was reduced in comparison to neat PVOH samples. The strain at break for PVOH reinforced with 0, 2.5, 5, and 10 % NFC were found to be 4.4, 3.2, 2.6, and 0.6, respectively. The lower strain at break of PVOH/NFC nanocomposites was probably due to the PVOH itself reaching its maximum tensile strength. Neat PVOH had the lowest value of ultimate tensile strength and tensile modulus, which were 16.1 and 25.5 MPa, respectively. As the amount of NFC increased, the ultimate tensile strength and tensile modulus increased.

Experimental data in this work were compared with theoretical models. For modeling mechanical properties of the composites, the tensile modulus of 100 % NFC was assumed to be that of a dried NFC film prepared by evaporating water from an NFC suspension. The NFC film was also punched out and tested using the same tensile testing conditions as the PVOH/NFC nanocomposites. The strain at break, tensile modulus, and ultimate tensile strength of dried NFC were 0.06, 3730 MPa, and 141.5 MPa, respectively. A comparison of tensile moduli is presented in Fig. 4. Theoretical modeling based on the modified rule of mixtures and percolation theory was in good agreement with experimental data. The rule of mixtures seemed to overestimate reinforcement phenomena. This could be due to the fact that the models assumed unidirectional and uniform fiber orientation and distribution in addition to a perfect bond between the matrix and the fiber (Bulota et al. 2011; Sharma 2002).

## Thermal properties

PVOH is a semicrystalline polymer in which high physical inter-chain and intra-chain interactions exist due to hydrogen bonding between hydroxyl groups. The introduction of nanosized cellulose fibers with hydroxyl groups alters the intra-molecular and inter-molecular interactions of the PVOH chains. This may affect both the crystallization behavior and the physical structure of PVOH, resulting in variations in properties of nanocomposite samples (Liu et al. 2007).

Because the PVOH degrades near its melting temperature (Tang and Alavi 2011; Marten 2002), three heating and two cooling cycles were performed so that useful comparisons could be made. Results from the initial heating cycle in DSC experiments were discarded because they included the latent heat from the water absorption in the samples.

### *Degradation*

Figures 5 and 6 show the second and third heating cycles, as well as the first and second cooling cycles, of PVOH and PVOH/NFC nanocomposites. As shown in Fig. 5, the endothermic peak, which occurred between 190 and 200 °C, is referred to as the melting peak of PVOH. An exothermic peak, which occurred between 160 and 180 °C, was observed in all specimens and corresponds to the crystallization of PVOH (cf. Fig. 6). Note that the additional thermal scanning cycles caused a decrease in the melting and crystallization temperatures as well as the heat, suggesting sample degradation (Probst et al. 2004; Holland and Hay 2001). The magnitude of the shift increased with

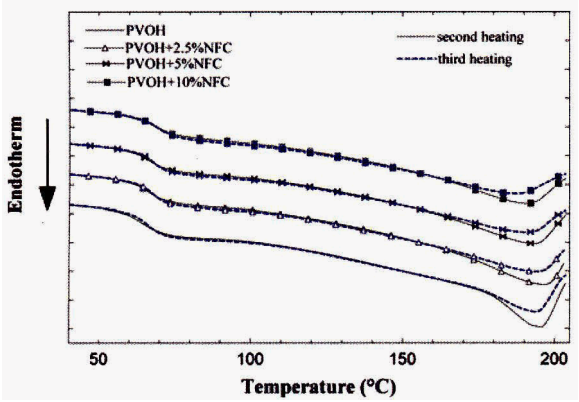


**Fig. 5** Comparison of the melting endotherms during the second (*solid line*) and third (*dashed line*) heating scans of PVOH and its nanocomposites with NFC

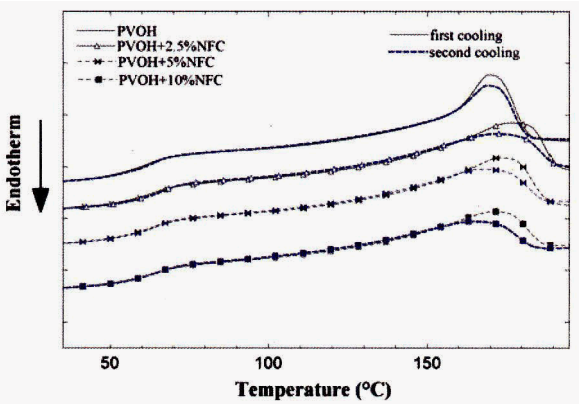


**Fig. 6** Comparison of the crystallization exotherms during the first (*solid line*) and second (*dashed line*) cooling scans of PVOH and its nanocomposites with NFC

increasing NFC concentration, indicating that NFC might cause degradation of the polymer, likely through residual moisture in NFC. This degradation was further confirmed by TGA results.

### *Nucleating effect*

Table 1 provides clear evidence that NFC also serves as a nucleating agent as the crystallization temperature ($T_c$) is higher with the addition of NFC. With the addition of 2.5 % NFC, the crystallization peak of PVOH is roughly 5 °C higher. Furthermore, the crystallization regime was prolonged as compared to neat PVOH. With further addition of NFC, however, the crystallization peak temperature decreased. The initial increase and then decrease of crystallization temperatures with increasing NFC content could be the result of several competing factors, including enhanced nucleation for crystallization, material degradation due to residual moisture in NFC, and/or physical interactions between the polymer and reinforcements that restrict the segmental mobility of the polymer chains. Similar effects by other nanosized materials on the crystallization and degradation of PVOH have been reported previously (Probst et al. 2004; Liu et al. 2007).

Furthermore, the enthalpy ($\Delta H$), percent crystallinity ($\chi_c$), and melting temperatures ($T_m$) calculated from the second cooling scan are shown in Table 1. The degree of crystallinity of PVOH was calculated based on the following equation,

$$\chi_c = \frac{\Delta H_m}{w\Delta H_m^0} \tag{8}$$

where $w$ is the weight fraction of PVOH in the composites, $\Delta H_m$ is the measured heat of fusion, and $\Delta H_m^0$ is the heat of fusion of a 100 % crystalline PVOH which has a value of 150 J/g (Finch 1973). As shown in Table 1, and similar to the change in crystallization temperature, the degree of crystallinity of PVOH increased slightly with a small addition of NFC, and then decreased. This increase in crystallinity is possibly due to the nucleating effect of the nanosized NFC fibers. The same phenomena were observed for tunicin whisker-reinforced plasticized starch (Mathew et al. 2008) and carbon nanotube-reinforced PVOH composites (Coleman et al. 2004). In addition, the shoulders in the DSC thermograms in Fig. 5 indicate

**Table 1 DSC results based on the second heating and first cooling scan**

| Samples | $T_g$ (°C) | $T_m$ (°C) | $\Delta H$ (J/g) | $X_c$ (%) | $T_c$ (°C) |
|---|---|---|---|---|---|
| PVOH | 66.2 | 195.4 | 12.0 | 8.0 | 168.1 |
| PVOH + 2.5 %NFC | 66.3 | 196.8 | 12.1 | 8.2 | 174.8 |
| PVOH + 5 %NFC | 66.6 | 193.1 | 11.2 | 7.8 | 171.2 |
| PVOH + 10 %NFC | 68.8 | 190.9 | 10.5 | 7.7 | 168.2 |

that the glass transition temperatures of PVOH and PVOH/NFC nanocomposite samples were between 50 and 80 °C.

## Thermal stability

The thermal stability of the neat PVOH and PVOH/NFC nanocomposite samples were examined using TGA. TGA results shown in Fig. 7 confirm that adding NFC leads to increased degradation. The onset degradation temperatures of the PVOH/NFC nanocomposites decreased with the addition of NFC.

As shown in Fig. 7, there was an initial and slow weight loss of NFC until around 200 °C, which might be attributed to both the loss of residual moisture in the NFC as well as the slow degradation of NFC. The most pronounced degradation began at approximately 200 °C, which was lower than the maximum temperature of 205 °C used in the heating scans during the DSC analysis. This supports the findings that the material might have degraded at the end of the first DSC heating scan (cf. Fig. 5). There was an approximate 30 % char yield at temperatures above 500 °C.

## Dynamic mechanical properties (DMA)

Since PVOH is a hydrophilic polymer, its properties were strongly affected by the presence of moisture in the samples (Bulota et al. 201 1; Roohani et al. 2008). For the study on the effects of moisture content in PVOH and NFC on the mechanical properties, two sets of specimens were prepared. The first set was removed from the 90 % humidity room and reconditioned for

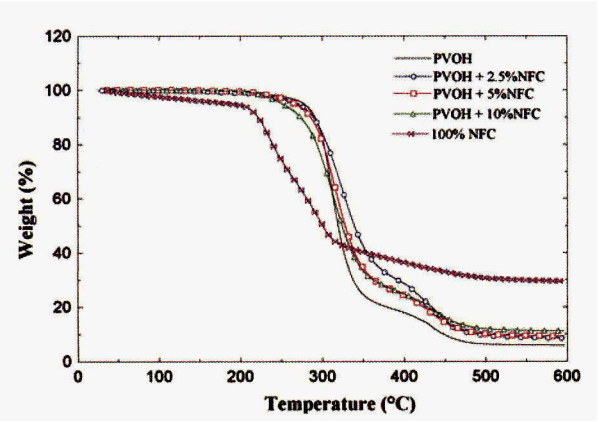


**Fig. 7** TGA curves for the PVOH/NFC nanocomposite samples

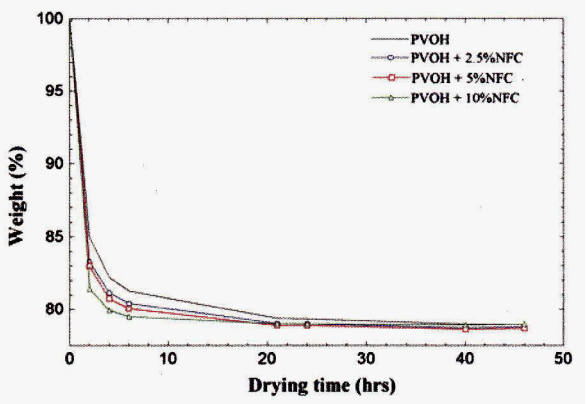


**Fig. 8** Weight of PVOH/NFC nanocomposites in a 90 % humidity room as a function of time as they were dried at 90 °C

4 days at 50 % humidity and 25 °C prior to testing. To further reduce the moisture content within the specimens, the other set of samples was dried at 90 °C for 2 days prior to the DMA test. Figure 8 shows the weight of PVOH/NFC nanocomposites, which were dried at 90 °C, from the 90 % humidity room as a function of time. The actual moisture contents of the samples from the 90 and 50 % humidity rooms were found to be around 21 and 7.5 %, respectively.

The logarithm of the storage modulus for PVOH nanocomposites prepared at the two moisture contents as a function of temperature are shown in Fig. 9. At low temperatures (−25 to 0 "C), it was difficult to observe any change in the storage modulus between the two moisture contents. In the glassy state, the tensile storage modulus, E, slightly decreased with temperature. Then, the modulus dropped at a temperature (around 25 or 50 °C) that depended on moisture conditioning. The modulus dropped earlier for samples that were conditioned at 50 % humidity and 25 °C. At 25 °C, high moisture content samples were soft and pliable but low moisture content samples led to a hard material (Roohani et al. 2008). Interestingly, for samples containing a lot of moisture and little or no NFC (Fig. 9a), the rubbery modulus was found to increase with temperature in the range of about 70–110 "C. This behavior might be caused by the loss of moisture during the DMA test. On the other hand, for dried samples (cf. Fig. 9b) at higher temperatures, the modulus dropped consistently. Regardless of the moisture content, the addition of NFC increased the rubbery modulus of the PVOH/NFC nanocomposites. Similar results have been

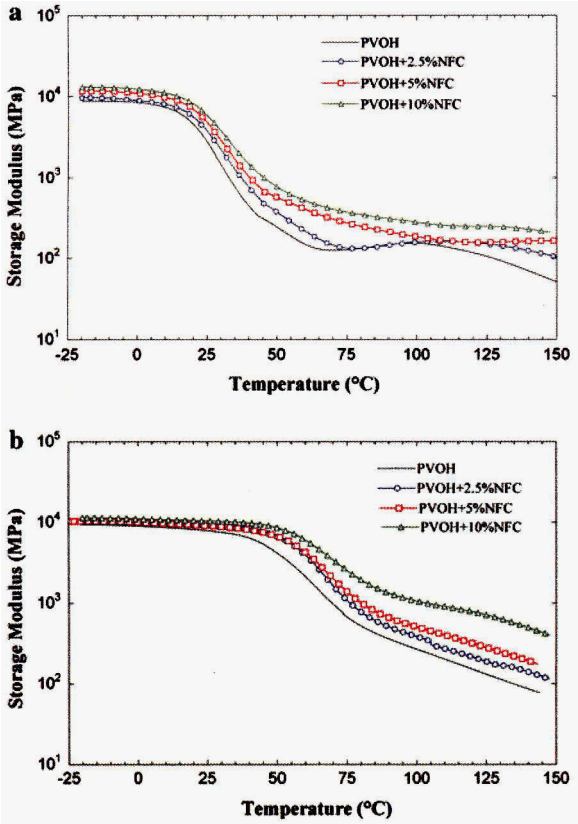


**Fig. 9** Storage moduli of the PVOH/NFC composite samples. a Samples were conditioned at 50 % humidity at 25 °C. b Samples were dried at 90 °C for 2 days

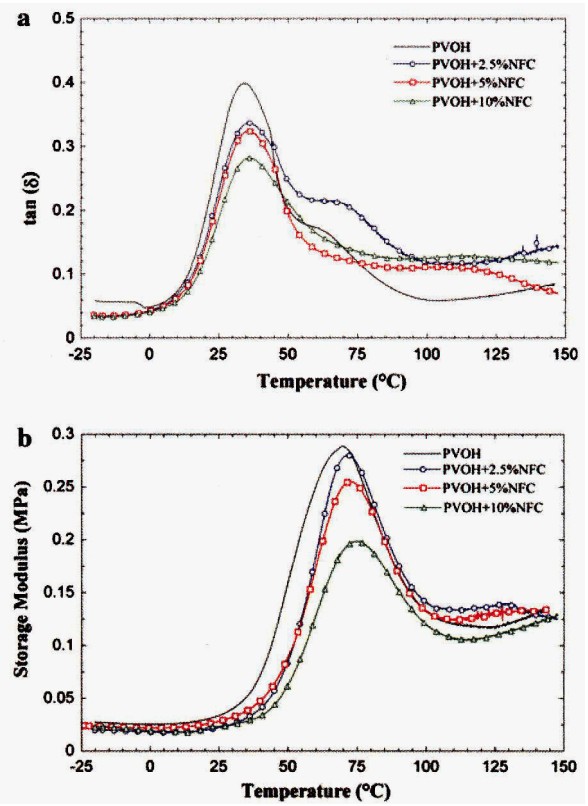


**Fig. 10** Tan-$\delta$ curves of the PVOH/NFC composite samples. a Samples were conditioned at 50 % humidity. b Samples were dried at 90 °C for 2 days

reported in other studies (Roohani et al. 2008; Lu et al. 2008).

The differences in mechanical properties can be attributed to the change in the glass transition temperature ($T_g$), which can be obtained from the peaks of the tan-b curves in Fig. 10. $T_g$ shifted to a lower temperature as the moisture content increased and plasticized the PVOH (Roohani et al. 2008). Moreover, a slight shift of the peak position was observed upon the addition of NFC, regardless of the moisture content. For samples conditioned at 50 % humidity, the peak position for PVOH was at 34.10 °C and increased to 36.05 °C for composites with 10 % NFC. Also, the magnitude of the relaxation process strongly decreased with increasing NFC content (Fig. 10). This indicates that fewer polymer chains participated in the transition. The increase in modulus, together with the positive shift in the tan-$\delta$ peak position, can be attributed to a physical interaction between the polymer and reinforcements that restricted the segmental mobility of the polymer chains in the vicinity of the nano-reinforcements (Javadi et al. 2010).

## Sorption behavior of $CO_2$ in PVOH nanocomposites

Cast PVOH and PVOH/NFC nanocomposite samples at two different moisture contents were originally weighed and then placed in a pressure vessel filled with $CO_2$ for 1 day. After depressurization, they were again placed on the scale to determine the amount of $CO_2$ absorbed and weight loss as a function of time. Samples with low moisture content absorbed little $CO_2$ and lost little weight as a function of time. Samples dried at 90 °C for 2 days did not gain any weight and the amount of $CO_2$ absorbed could not be detected. However, PVOH and PVOH/NFC nanocomposite samples with high moisture content (i.e., those from the 90 % humidity room) absorbed much more $CO_2$ due to the increased permeability of PVOH to $CO_2$ with moisture. This same observation was

reported in other studies (Piringer and Baner 2000; Marten 2002; Brandrup et al. 1999). For the sake of brevity, only samples conditioned at 90 % humidity are presented.

Figure 11 shows a plot of the measured solubility of $CO_2$ (%) in PVOH and PVOH/NFC nanocomposites. Note that the solubility of $CO_2$ in the specimens decreased as the NFC content increased because NFC, which has high crystallinity, does not absorb $CO_2$ as reported by number of studies (Doroudiani et al. 2002; Rachtanapun et al. 2003; Matuana et al. 1998). Neat PVOH was found to have around 3 % $CO_2$ solubility. With the addition of 10 % NFC, the apparent solubility of $CO_2$ decreased by as much as 33 %, which was much higher than the 10 % that might be expected. The additional reduction in weight gain might be because of faster gas loss while depressurizing the chamber and transferring the specimens to the scale. Accelerated weight loss with the addition of NFC was confirmed by desorption measurements.

The desorption curves for $CO_2$ in the neat PVOH and PVOH/NFC nanocomposite samples around one to 2 h are illustrated in Fig. 12. There is around 40 s delay after depressurizing and before weighing. The weight loss during this short period of time can be estimated by extrapolating the relatively flat mass loss curves at time equals zero. The additional mass losses for all of the samples were found to be less than 2.5 % of the total mass uptake. Note that the samples were weighed in an oil bath on the scale. Since it takes time for the $CO_2$ gas to pass through the oil to the atmosphere, there is a short lag time in the weight change. Thereafter, the slope became steeper as the NFC content increased, especially for the PVOH + 10 % NFC specimen. Hence, the desorption diffusivity became higher as the amount of NFC

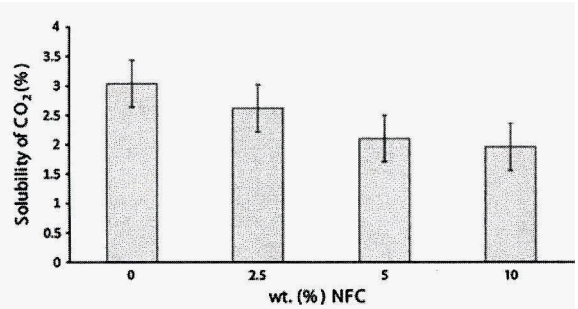


**Fig. 11** Solubility of $CO_2$ in PVOH and their nanocomposites with 2.5, 5, and 10 wt% NFC

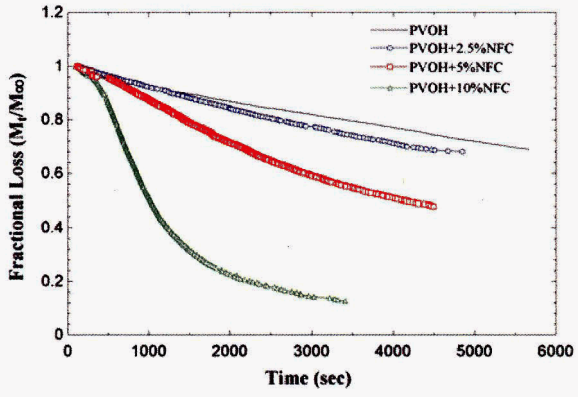


**Fig. 12** Desorption curves for $CO_2$ in PVOH and PVOH/NFC nanocomposites during the first hour; $M_t$ is the amount of gas lost at time $t$ and $M_\infty$ is the mass uptake at infinite time

increased. The increase in desorption diffusivity with increasing fiber content might be due to the interface between the fibers and the matrix which could provide a channel through which gas can quickly escape from the composites as reported in (Doroudiani et al. 2002; Rachtanapun et al. 2003).

## Foamed PVOH/NFC nanocomposites

To investigate their foaming behavior, specimens were placed in hot oil after removal from the $CO_2$ pressure vessel. Both specimens that were conditioned at 90 % humidity or dried prior to placement in the pressure vessel were investigated. Dried PVOH nanocomposite samples did not appear to foam at the conditions used (Fig. 13). On the other hand, at a high moisture content, some small cells can be clearly seen in the neat PVOH (Fig. 14a). These cells are believed to be caused by $CO_2$ with moisture plasticizing the films, which can lower the resistance to gas cell growth (Zhu et al. 2010; Kumar and Nadella 2004). Note that there were no visible cells found in the PVOH/NFC nanocomposites. This is probably because the nanocomposites had a higher strength at room temperature (Fig. 9a), which could hinder cell growth and reduce cell size (Lee et al. 2005).

Figure 15 shows the SEM micrographs from the center portion of the cross-section of the tensile bars after foaming in a hot oil bath at 135 °C for 10 s. The cell size found in the neat PVOH in Fig. 14a increased with the hot oil treatment. This was due to the moisture vapor that was generated at the oil bath temperature and diffused into the cells, enlarging

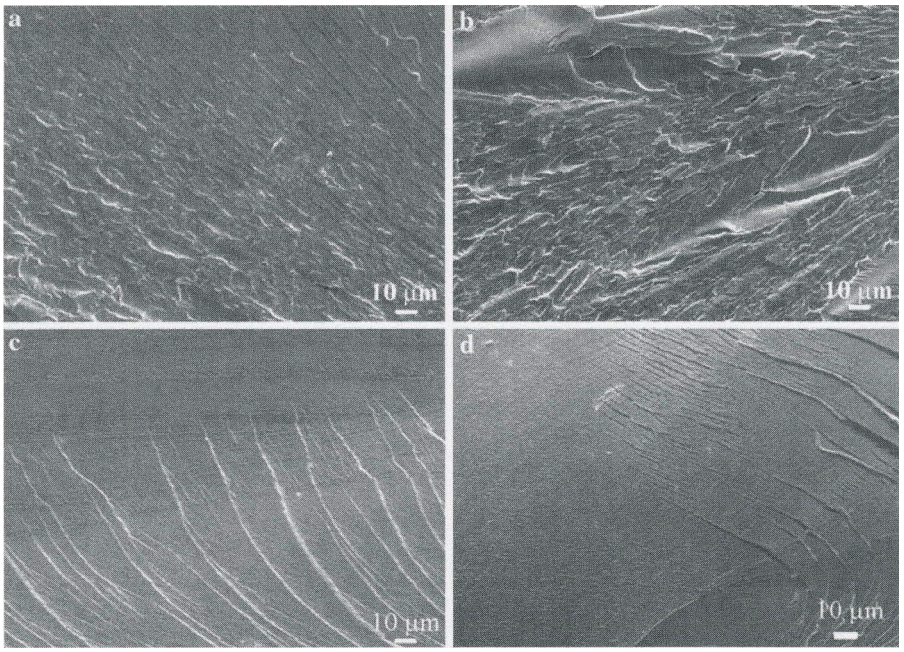


**Fig. 13** SEM images of dried PVOH and PVOH/NFC nanocomposites after they were placed into a $CO_2$ pressure vessel and subjected to a rapid pressure drop and hot oil treatment: **a** PVOH, **b** PVOH + 2.5 % NFC, **c** PVOH + 5 % NFC, and **d** PVOH + 10 % NFC. No visible foaming was observed

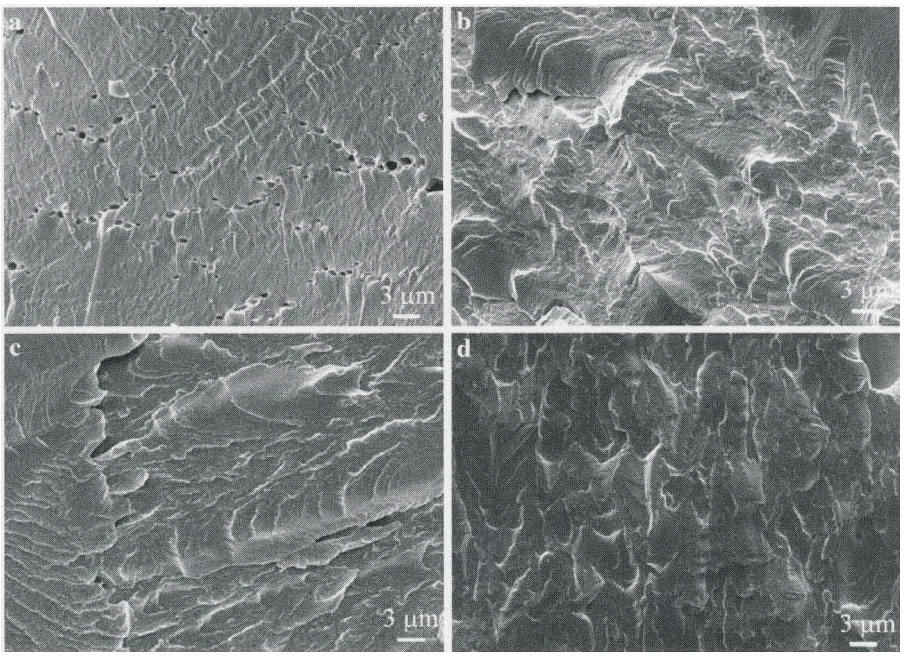


Fig. 14 SEM images of high moisture content PVOH and PVOH/NFC nanocomposites after they were placed into a CO2 pressure vesel and subjected to a rapid pressure drop at room temperature **a** PVOH, **b** PVOH + 2/5 % MFC. **c** PVOH + 5 % NFC, and **d** PVOH + 10 % MFC

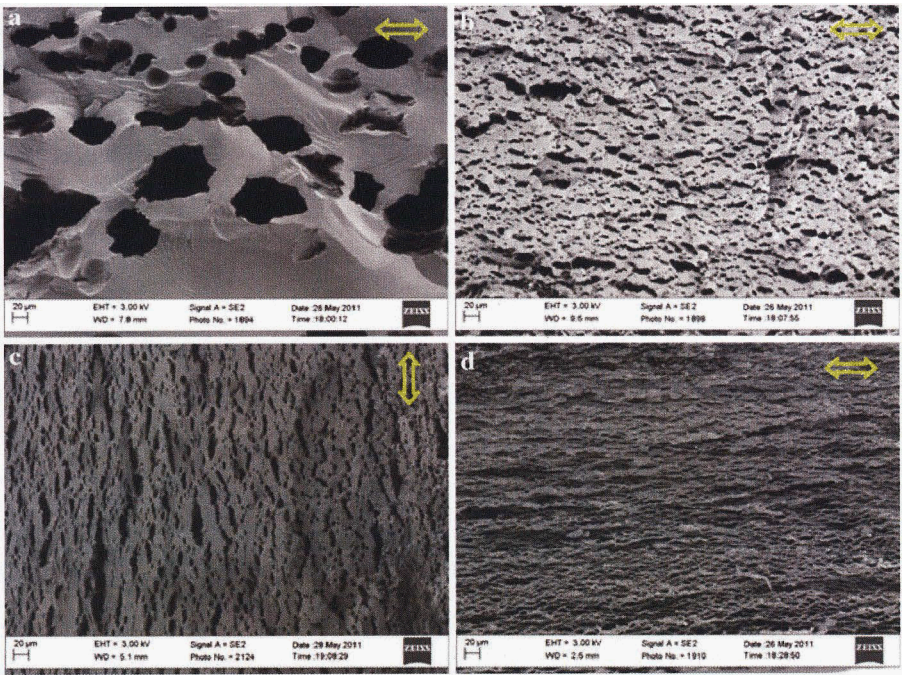


**Fig. 15** SEM images of high moisture content PVOH and PVOH nanocomposites foamed after hot oil treatment: **a** PVOH, **b** PVOH + 2.5 % NFC, **c** PVOH + 5 % NFC, and **d** PVOH + 10 % NFC. *Arrows* indicate the planar direction (the long axis and width directions of the sample) of the sample

them. Furthermore, a greater number of cells formed in the PVOH/NFC nanocomposites. The reasons for the formation of these cavities in the PVOH/NFC nanocomposites is probably due to very small cells that were created after depressurization but that could not be seen at the magnification in Fig. 14b–d; the evaporation of moisture in the samples could enlarge these cells. In general, placing samples into the $CO_2$ pressure vessel for 1 day prior to depressurization helped to pre-condition the samples and generate small cells as nuclei. Subsequently, placing them into a hot oil bath allowed the moisture in the samples to evaporate and expand the pre-existing cell nuclei into a system of dense cells. Without $CO_2$ pre-conditioning, the moisturized sample exhibited severe cracking in the hot oil bath.

The average cell size of the neat foamed PVOH was 32.6 μm and the cell morphology seemed more isotropic (Fig. 16). For PVOH/NFC nanocomposites, the cells became less uniform and more extended in the planar directions (the long axis and width directions of the sample). This was probably due to the preferable orientation of NFC fibers parallel to the film surface that hampered gas diffusion and cell growth in the thickness direction. In addition, cell size in the PVOH/NFC nanocomposites generally decreased with increasing NFC content and the cell density

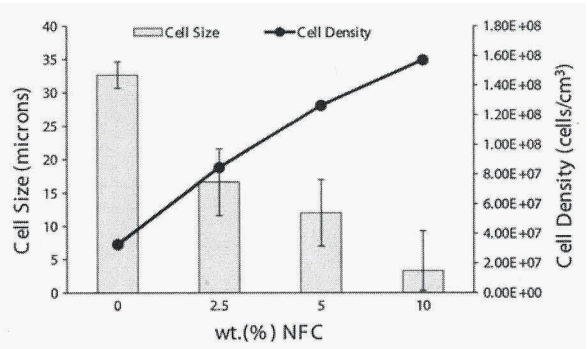


**Fig. 16** The average cell size and cell density of foamed PVOH nanocomposites

increased, suggesting that NFC nucleates cells. These results agree with findings from the literature on other types of nanocomposites (Chandra et al. 2005; Yuan et al. 2005; Gong et al. 2005). It should be pointed out that a few larger cells observed in the PVOH/NFC nanocomposites were likely formed by evaporated vapor from the NFC instead of $CO_2$, thus resulting in a large error bar. The densities of the solid neat PVOH and PVOH/NFC nanocomposites were all around 1,310 kg/m$^3$, and that of the foamed samples were 1,082, 1,102, 1,050, and 1120 kg/m$^3$ for PVOH, PVOH + 2.5 % NFC, PVOH + 5 % NFC, and PVOH + 10 % NFC, respectively.

### Tensile properties of foamed PVOH nanocomposites

Tensile tests were performed on the foamed specimens of the PVOH/NFC nanocomposites (cf. Fig. 17). The specific Young's modulus was obtained by dividing the modulus by the density.

As shown in Fig. 17a, the addition of NFC increased the specific Young's modulus of both solid and foamed samples significantly. The specific Young's modulus of the foamed specimens was generally higher than that of their solid counterparts but there was no significant difference in the specific strength (Fig. 17b). However, the strain-at-break (Fig. 17c) of the foamed specimens was lower. This can be attributed to the presence of large cells that served as stress concentrators in the foamed samples (Kramschuster et al. 2007).

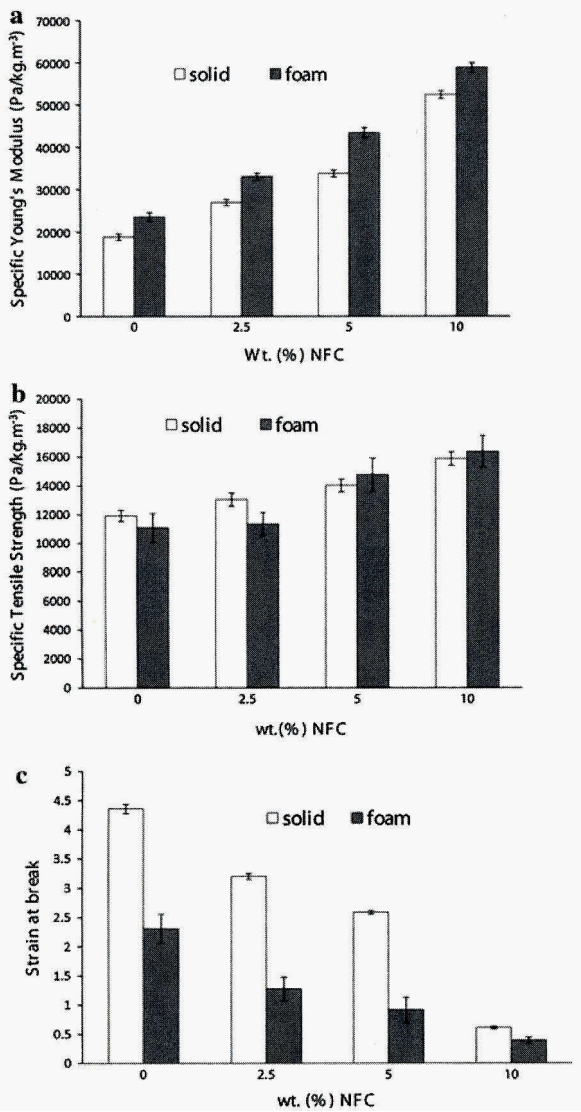


**Fig. 17** Specific mechanical properties of solid and foamed PVOH/NFC nanocomposites: **a** specific Young's modulus (Pa/kg $m^3$), **b** specific tensile strength (Pakg $m^{-3}$), and **c** strain at break

## Conclusions

NFC dispersed well in PVOH by blending a suspension of NFC with a solution of PVOH. PVOH/NFC nanocomposite films were then formed by a casting/evaporation technique. NFC had a reinforcing effect on PVOH, as observed via both DMA and tensile tests. However, toughness decreased as the amount of NFC increased. The addition of NFC to PVOH was shown to increase the crystallization and glass transition temperatures, but it also caused thermal degradation of the polymer, likely due to an increase in moisture. The sorption degree of $CO_2$ in the nanocomposites was dependent on the moisture content in the samples as solubility increased with higher moisture contents. The solubility was around 3 % in neat PVOH conditioned at 90 % humidity and decreased as the amount of NFC increased. Moreover, the desorption diffusivity increased as more NFC was added. The moisture in the neat PVOH and PVOH/NFC nanocomposites acted as a plasticizer and enabled foaming by a batch foaming process. In addition, vapor that came from the evaporation of moisture in the samples also acted as a physical blowing agent by diffusing into the cells and enlarging them. Finally, the addition of NFC increased cell density and decreased cell size in moisture-enabled foamed PVOH/NFC nanocomposites.

**Acknowledgments** The financial support of the United States Department of Agriculture National Institute of Food and Agriculture Award (No. 201 1-67009-20056) is gratefully acknowledged in this research. The authors would also like to thank Dr. Srikanth Pilla for his useful suggestions, Dr. Tom Kuster of the Forest Products Laboratory for performing electron microscopy, and Dr. Rick Reiner of the Forest Products Laboratory for preparing cellulose nanofibers.

## References

Ahola S (2008) Properties and interfacial behaviour of cellulose nanofibrils. Dissertation, Helsinki University of Technology

Alemdar A, Sain M (2008) Isolation and characterization of nanofibers from agricultural residues-Wheat straw and soy hulls. Bioresour Technol 99:1664–1671

Allen G, Bowden M, Todd S, Blundell D, Jeffs G, Davies W (1974) Composites formed by interstitial polymerization of vinyl monomers in polyurethane elastomers: 5. Variation of modulus with composition. Polymer 15:28–32

Andresen M, Johansson LS, Tanem BS, Stenius P (2006) Properties and characterization of hydrophobized microfibrillated cellulose. Cellulose 13:665–677

ASTM D638-10 (2010) Standard test method for tensile properties of plastics. ASTM International, West Conshohocken, PA. doi:10.1520/D0638-10

ASTM D792-08 (2008) Standard test methods for density and specific gravity (relative density) of plastics by displacement, ASTM International, West Conshohocken, PA

Avella M, Cocca M, Errico M, Gentile G (2011) Biodegradable PVOH-based foams for packaging applications. J Cell Plast 47:271

Brandrup J, Immergut EH, Grulke EA (1999) Polymer handbook. Wiley, New York

Bulota M, Jääskeläinen A, Paltakari J, Hughes M (2011) Properties of biocomposites: influence of preparation method, testing environment and a comparison with theoretical models. J Mater Sci 46:3387–3398

Chandra A, Gong S, Yuan M, Turng LS, Gramann P, Cordes H (2005) Microstructure and crystallography in microcellular injection molded polyamide 6 nanocomposite and neat resin. Polym Eng Sci 45:52–61

Coleman JN, Cadek M, Blake R, Nicolosi V, Ryan KP, Belton C, Fonseca A, Nagy JB, Gun'ko YK, Blau WJ (2004) High performance nanotube-reinforced plastics: understanding the mechanism of strength increase. Adv Funct Mater 14:791–798

Davies W (1971a) The elastic constants of a two-phase composite material. J Phys D Appl Phys 4:1176

Davies W (1971b) The theory of composite dielectrics. J Phys D Appl Phys 4:318

Doroudiani S, Chaffey CE, Kortschot MT (2002) Sorption and diffusion of carbon dioxide in wood-fiber/polystyrene composites. J Polym Sci Pol Phys 40:723–735

Dufresne A, Cavaillé JY, Vignon MR (1997) Mechanical behavior of sheets prepared from sugar beet cellulose microfibrils. J Appl Polym Sci 64:1185–1194

Finch CA (1973) Polyvinyl alcohol: properties and applications, vol 339. Wiley, New York

Gong S, Yuan M, Chandra A, Kharbas H, Osorio A, Turng L (2005) Microcellular injection molding. Int Polym Proc 20:202–214

Holland B, Hay J (2001) The thermal degradation of poly (vinyl alcohol). Polymer 42:6775–6783

Iwamoto S, Nakagaito A, Yano H (2007) Nano-fibrillation of pulp fibers for the processing of transparent nanocomposites. Appl Phys A Mater 89:461–466

Javadi A, Srithep Y, Lee J, Pilla S, Clemons C, Gong S, Turng LS (2010) Processing and characterization of solid and microcellular PHBV/PBAT blend and its RWF/nanoclay composites. Compos Part A Appl S 41:982–990

Jonoobi M, Harun J, Mathew AP, Oksman K (2010) Mechanical properties of cellulose nanofiber (CNF) reinforced polylactic acid (PLA) prepared by twin screw extrusion. Compos Sci Technol 70:1742–1747

Kramschuster A, Gong S, Turng LS, Li T (2007) Injection-molded solid and microcellular polylactide and polylactide nanocomposites. J Biobased Mater Bio 1:37–45

Kumar V, Nadella KV (2004) Microcellular foams. In: Eaves D (ed) Handbook of polymer foams. Smithers Rapra Press, Shropshire, pp 243–268

Labuschagne PW, Germishuizen WA, Verryn SMC, Moolman FS (2008) Improved oxygen barrier performance of poly (vinyl alcohol) films through hydrogen bond complex with poly (methyl vinyl ether-co-maleic acid). Eur Polym J 44:2146–2152

Lee LJ, Zeng C, Cao X, Han X, Shen J, Xu G (2005) Polymer nanocomposite foams. Compos Sci Technol 65:2344–2363

Liu M, Guo B, Du M, Jia D (2007) Drying induced aggregation of halloysite nanotubes in polyvinyl alcohol/halloysite nanotubes solution and its effect on properties of composite film. Appl Phys A Mater 88:391–395

Lu J, Wang T, Drzal LT (2008) Preparation and properties of microfibrillated cellulose polyvinyl alcohol composite materials. Compos A 39:738–746

Marten FL (2002) Vinyl alcohol polymers. Kirk-Othmer Encycl Chem Technol. doi:10.1002/0471238961.2209142513011820

Mathew AP, Thielemans W, Dufresne A (2008) Mechanical properties of nanocomposites from sorbitol plasticized starch and tunicin whiskers. J Appl Polym Sci 109:4065–4074

Matuana LM, Park CB, Balatinecz JJ (1998) Cell morphology and property relationships of microcellular foamed pvc/wood-fiber composites. Polym Eng Sci 38:1862–1872

Naguib HE, Park CB, Panzer U, Reichelt N (2002) Strategies for achieving ultra low density polypropylene foams. Polym Eng Sci 42:1481–1492

Nakagaito A, Yano H (2004) The effect of morphological changes from pulp fiber towards nano-scale fibrillated cellulose on the mechanical properties of high-strength plant fiber based composites. Appl Phy A Mater 78:547–552

Osswald TA (2006) International plastics handbook: the resource for plastics engineers. Hanser, Verlag

Piringer OG, Baner AL (2000) Plastic packaging materials for food: barrier function, mass transport, quality assurance, and legislation. Wiley-Vch, Weinheim

Poling BE, Thomson GH, Friend DG, Rowley RL, Wilding WV (2008) Perry's chemical engineer's handbook. McGraw-Hill, New York

Probst O, Moore EM, Resasco DE, Grady BP (2004) Nucleation of polyvinyl alcohol crystallization by single-walled carbon nanotubes. Polymer 45:4437–4443

Rachtanapun P, Selke S, Matuana L (2003) Microcellular foam of polymer blends of HDPE/PP and their composites with wood fiber. J Appl Polym Sci 88:2842–2850

Roohani M, Habibi Y, Belgacem NM, Ebrahim G, Karimi AN, Dufresne A (2008) Cellulose whiskers reinforced polyvinyl alcohol copolymers nanocomposites. Eur Polym J 44:2489–2498

Saito T, Okita Y, Nge T, Sugiyama J, Isogai A (2006) TEMPO-mediated oxidation of native cellulose: microscopic analysis of fibrous fractions in the oxidized products. Carbohydr Polym 65:435–440

Samir MASA, Alloin F, Dufresne A (2005) Review of recent research into cellulosic whiskers, their properties and their application in nanocomposite field. Biomacromolecules 6:612–626

Sanchez-Garcia MD, Lagaron JM (2010) On the use of plant cellulose nanowhiskers to enhance the barrier properties of polylactic acid. Cellulose 17:987–1004

Sharma S (2002) Economics of composites and reinforcements. Composite materials, 1st edn. Narosa Publishing House, New Delhi, pp 20–25

Siqueira G, Bras J, Dufresne A (2010) Cellulosic bionanocomposites: a review of preparation, properties and applications. Polymers 2:728–765

Siró I, Plackett D (2010) Microfibrillated cellulose and new nanocomposite materials: a review. Cellulose 17:459–494

Stern S, Shah V, Hardy B (1987) Structure-permeability relationships in silicone polymers. J Polym Sci Pol Phys 25: 1263–1298

Syverud K, Stenius P (2009) Strength and barrier properties of MFC films. Cellulose 16:75–85

Tang X, Alavi S (2011) Recent advances in starch, polyvinyl alcohol based polymer blends, nanocomposites and their biodegradability. Carbohydr Polym 85:7–16

Yuan M, Winardi A, Gong S, Turng LS (2005) Effects of nano and micro fillers and processing parameters on injection molded microcellular composites. Polym Eng Sci 45:773–788

Zhu B, Zha W, Yang J, Zhang C, Lee LJ (2010) Layered-silicate based polystyrene nanocomposite microcellular foam using supercritical carbon dioxide as blowing agent. Polymer 51:2177–2184